EFFECT OF THE SOLIDIFICATION FRONT VELOCITY ON THE MICROSTRUCTURE OF THE EUTECTIC IN A HYPEREUTECTIC AL-SI ALLOY

Éva Kócsák
MSc metallurgical engineering student, University of Miskolc, FKNI
3515 Miskolc-Egyetemváros, e-mail: kocsak.eva@student.uni-miskolc.hu

Arnold Rónaföldi
titular university professor, University of Miskolc, FKNI
3515 Miskolc-Egyetemváros, e-mail: rarnold@digikabel.hu

András Roósz
Professor Emeritus, University of Miskolc, FKNI
3515 Miskolc-Egyetemváros, e-mail: femroosz@uni-miskolc.hu

Zsolt Veres
associate professor, University of Miskolc, FKNI
3515 Miskolc-Egyetemváros, e-mail: zsolt.veres@uni-miskolc.hu

Abstract

The aluminium-silicon (Al-Si) alloys are widely used, and in combination with the appropriate mechanical properties, they are attractive raw materials even for the automobile and aircraft industries. Its eutectic has an irregular structure, which makes its classification challenging. The silicon phase of the eutectic has a lamella morphology, which can be modified by various interventions. Their microstructure can be influenced by changes in solidification parameters, such as flows induced by a rotating magnetic field (RMF) (Li et al., 2020), changes in the movement velocity of the solidification front (Zimmermann et al., 2005), and changes in the temperature gradient (Li et al., 2018). During our work, we dealt with an Al–Si 18% hypereutectic alloy stirred (7.2 mT) and not stirred by the rotating magnetic field. The experiments were performed at different sample moving velocities, and the eutectic of the samples was examined using image analysis software.

Keywords: *solidification, RMF, aluminium-silicon alloy*

1. Introduction

Hypereutectic Al-Si alloys are occurring in increasing numbers in the aircraft industry and automotive. The wide application range of hypereutectic alloys is due to properties such as good thermal and electrical conductivity, high strength, and good corrosion resistance. The high Si content increases the volume of the primary Si and the hardness of the alloy but reduces the machinability. (Miladinović et al., 2023) Grain refinement is necessary to improve the properties and meet the industry's high expectations. The tested samples had a silicon content of 18 wt%. In this case, primary silicon first solidified from the melt during cooling and then eutectic (Matsuura et al., 2003) *(Figure 1)*.

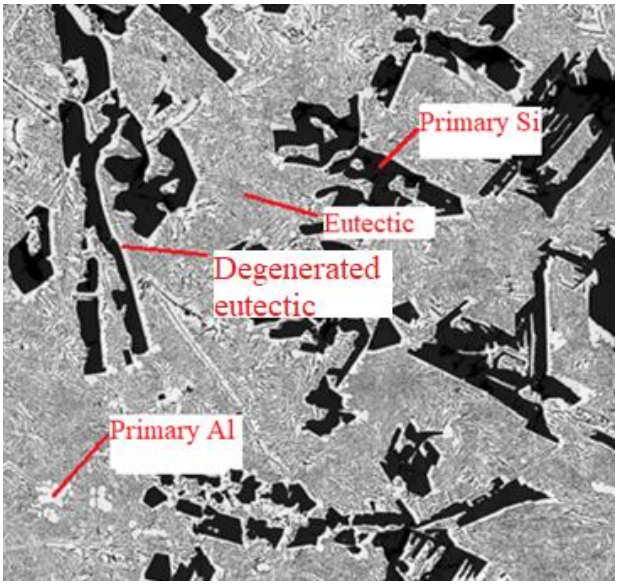

Figure 1. *Microstructure of a solidified Al18Si alloy, M = 500*

The primary silicons that first solidify in the hypereutectic Al-Si alloy appear in varied forms. In terms of their shape, they can be, among others, polyhedral *(Figure 1)*, star-like (Pei et al., 2001) or dendritic (Toropova et al., 2022) *(Figure 2)*. In addition to the differences in shape, their size can also be quite different.

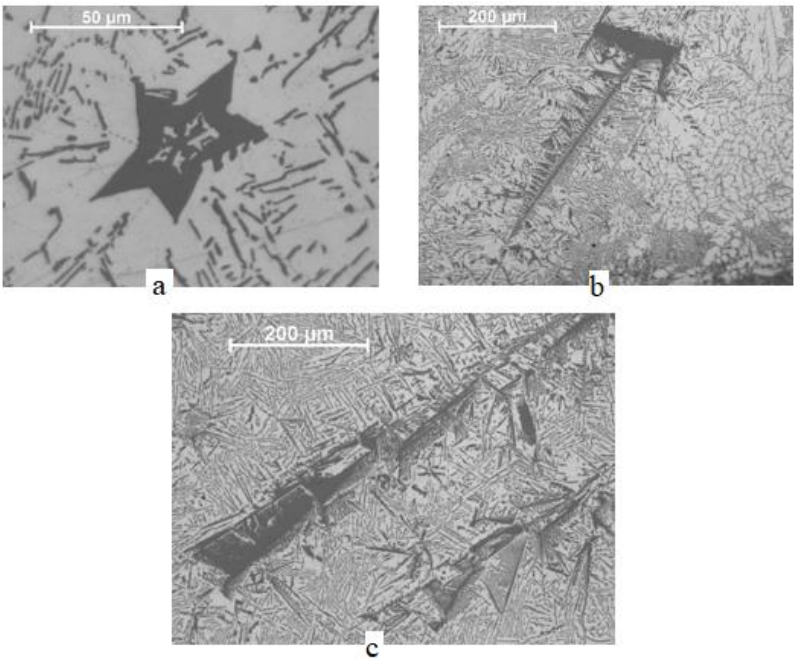

Figure 2. *Some examples of the morphology of primary Si, M = 500*
a: star-like; b: dendritic, c: feather-like (a special type of dendrites)

Day and Hellawell have discussed the growth mechanism of silicon in the Al-Si eutectic alloy under different solidification conditions, among others. The morphology of silicon lamellas of the eutectic Al-Si alloy was investigated as a function of the temperature gradient and the front movement velocity.

The front movement velocity (vs/l) [mm/s] can be understood as the velocity of the movement of the solidification front in the melt, so a velocity of the advance of the solid/melt interface. The high interfacial velocity means less time is available for equilibrium growth. So, the bigger interface velocity causes a finer structure. The cooling velocity can be measured based on the thermal gradient and the interface velocity.

A total of three different mechanisms were presented by Day and Hellawell. At velocities less than 5 μm/s, the preferred growth direction of the primer Si is <100>, and the shapes change from relatively uniform, closely spaced rods to various rough shapes as the temperature gradient decreases. At a higher front velocity of up to 1 mm/s, silicon occurs in a star shape and is only approximately aligned with the growth direction. At velocities above 1 mm/s, the silicon will be characterised by an irregular, often branched structure (Day et al., 1968). During the solidification of metals – under terrestrial conditions – flows are generated in the melt. Their effect can also be investigated by creating excited flows of different intensities in the melt, which ultimately affect the structure of the solidified metal (Holmes et al., 2005; Cadirli et al., 2015; Chen et al., 2010).

Zimmermann and Weiss (Zimmermann et al., 2005) report two flows when RMF is applied. The primary flow is produced by the Lorentz force, and the secondary flow is generated by the centrifugal force and the radial pressure gradient near the horizontal walls. The velocity of the secondary flow is approximately ten times less than the velocity of the primary flow. As a result of combining these two flows, a spiral-shaped flow is created, which influences the solidification.

2. Experiments

The experiments were carried out in a Bridgman-type tube furnace with 4 heating zones. The drawing of the equipment can be seen in *Figure 3*.

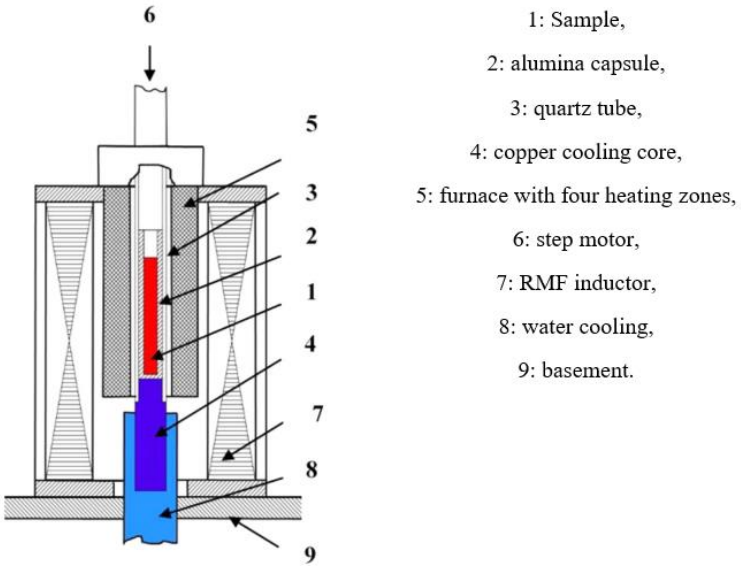

Figure 3. *Sketch of the solidification facility* (Veres et al., 2022)

The heating zones can be controlled independently to achieve the desired temperature distribution along the length of the furnace. The samples were moved down into the water-cooling chamber during solidification using the step motor. We had 5 different experiments with the samples. The movement velocity of the samples was different according to the following: Sample A had 0.02 mm/s, Sample B had 0.05 mm/s, Sample C had 0.1 mm/s, Sample D had 0.2 mm/s, and Sample E had 0.5 mm/s movement velocity. The sample used in the equipment has a diameter of 8 mm and a length of 120 mm. The samples were placed in an alumina capsule. During the experiments, the solidification took place in a controlled manner, so the solidification was unidirectional. The first half of the samples was solidified without using RMF, while the second part was solidified using RMF. In this case, it became possible to investigate the differences between the transitions and the stirred parts as a function of the movement velocity. We can also see what the microstructure of the sample looks like when the RMF is turned on, and structural changes occur.

In each case, there were 2 halves of the 5 available solidified samples, the stirred and unstirred half. In order for transitions to be studied and structural differences to be detected, each sample was divided into 6 equal parts. The locations marked on the samples can be marked with the following length dimensions *(Table 1)*.

Table 1

The 6 investigated locations of the samples

Place	Distance from the beginning of the sample
1	0 mm - 20 mm
2	20 mm - 40 mm
3	40 mm - 60 mm
4	60 mm - 80 mm
5	80 mm - 100 mm
6	100 mm - 120 mm

In these parts, the eutectic was measured at 50× magnification. The low-magnification image includes half of the sample, and we can perform macro analyses on these images because the primary silicons are well separated from the eutectic *(Figure 4)*.

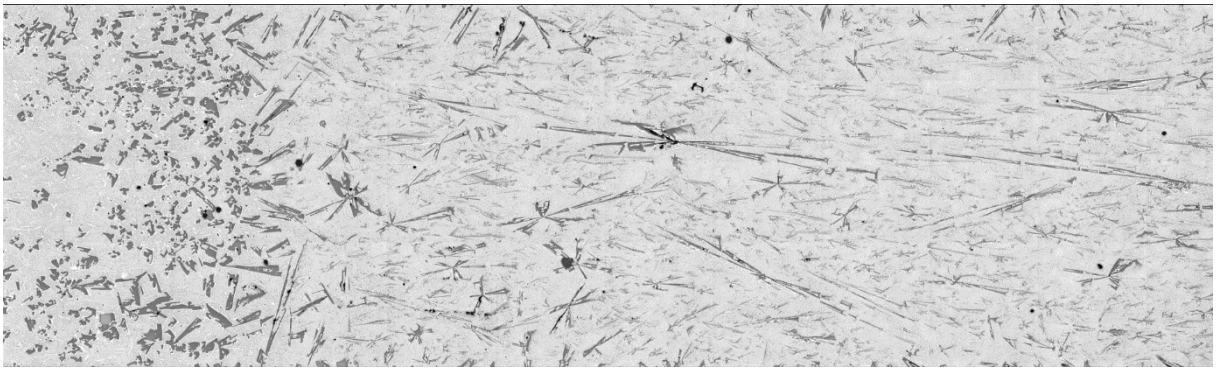

Figure 4. *Microscopic image of Al18Si, movement velocity 0.02 mm/s, unstirred part, M: 50×*

In addition, mosaic images of higher resolution, 10 × 20 frames and 500×magnification were created from these parts *(Figure 5)*. Due to the higher resolution, the two phases of the eutectic are already separated, so the images are suitable for examining the silicon lamellas in the eutectic. Images were taken with a Zeiss AXIO Imager M1M light microscope.

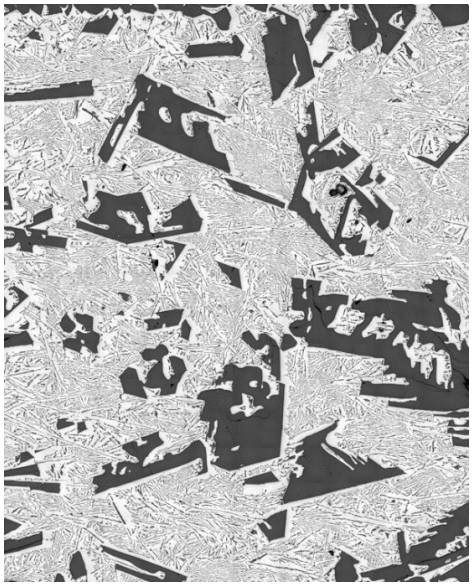

Figure 5. *Microscopic image of Al18Si, movement velocity 0.02 mm/s, unstirred part, M: 500×*

The results were evaluated in the following order:

1. We measure the area of the primary silicon in each piece, which, if we subtract it from the total area of the image, gives us the area of the eutectic, and then we can calculate the ratio from this. Since the pictures were taken in black and white, the Image J program can separate the primer silicon (black) and the eutectic (white aluminium, with grey silicon lamellas) according to grey level.
2. Examining the length of the silicon lamellas in the eutectic and measuring their relative distance. After the quantitative measurement of the eutectic and primary silicon, the silicon lamellas in the eutectic were investigated. This included measuring the average distance between the lamellas, which is a challenge from the point of view of the irregular structure of the Al-Si alloy. We worked with the largest Feret diameter in all cases during the investigation. As a result, introducing a method was essential, making the average distance between the silicon lamellas numerically measurable, thus allowing us to determine the fineness of the eutectic structure. Thus, the relationship between the average distance between lamellas:

$$\lambda_a = 2 * \frac{\mathrm{Ap} * (1 - A_f)}{N * P_0} \tag{1}$$

where,

- P_0: the average circumference of the Si lamellas in the examined light microscope image [μm];
- N: number of eutectic lamellas;
- A_p: area of the microscopic image (μm^2);
- A_f: fraction of the area of the eutectic lamellas in the eutectic structure.

3. Results and discussion

The determination of the average eutectic amount of the entire piece can be seen in *Figure 6*. Typically, a similar eutectic volume increase occurred at all movement velocities.

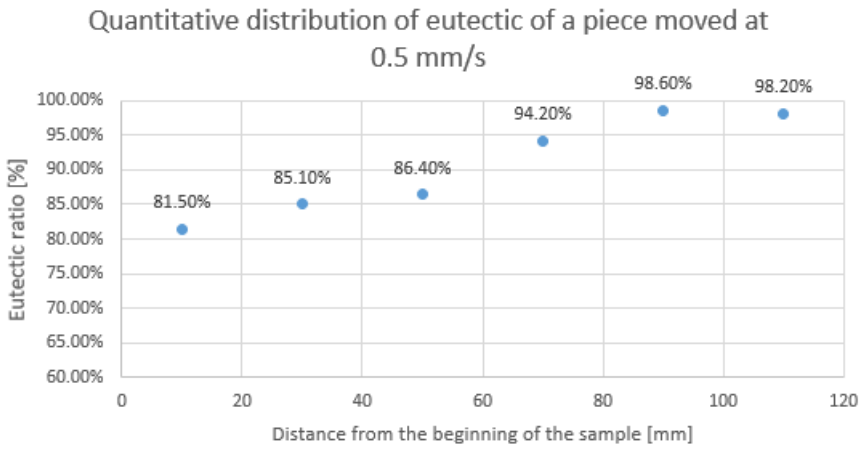

Figure 6. *Change in the amount of eutectic in sample 0.5 mm/s movement velocity*

In *Figure 7*, we can see the amount of eutectic formed by changing the movement velocity at the beginning, middle and end of each sample.

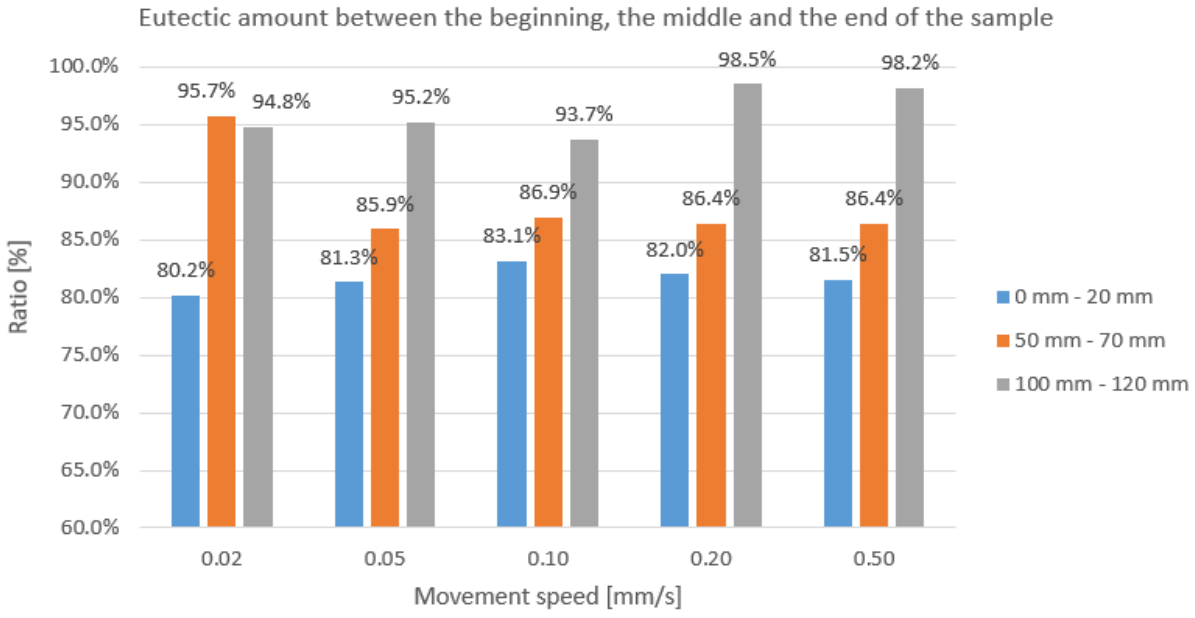

Figure 7. *Change in the amount of eutectic as a function of movement velocities*

We can state that the amount of eutectic in the unstirred part of the samples is around 85%, which is an average 8% decrease in the amount of eutectic compared to the equilibrium (calculated) state (93.82%).

This decrease is because typically, all samples are enriched downward in silicon, so primary silicon appears in large quantities in the first one-sixth of the samples. For this reason, the amount of eutectic in the area between 0 mm–20 mm is 10-15% less than in the areas between 100 mm–120mm *(Figure 8)*.

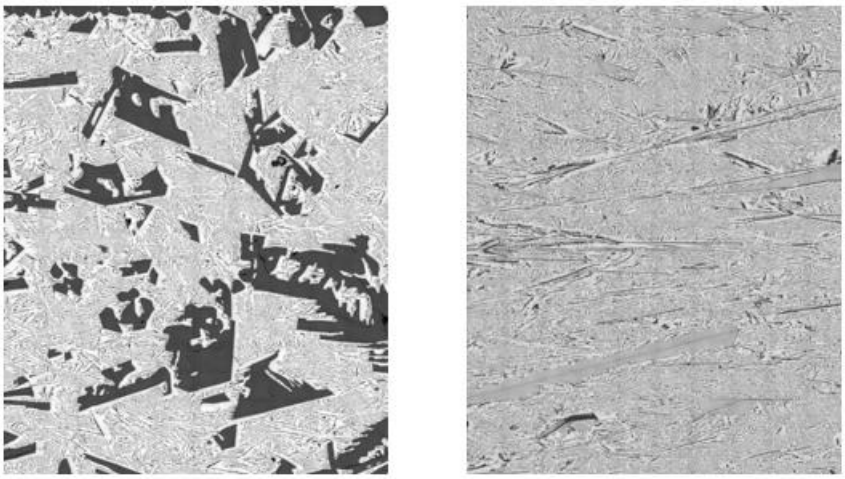

Figure 8. *Microscopic image of Al18Si, movement velocity 0.02 mm/s, a. area 0 mm–20 mm, b. 100 mm–120 mm, M: 500×*

Depending on the movement velocity values in the stirred parts of the samples, the amount of eutectic decreases up to a medium movement velocity and then increases compared to the equilibrium state. This is presumably because by increasing the movement velocity, the supercooling of silicon takes place in different asymmetric coupled zones *(Figure 9)*.

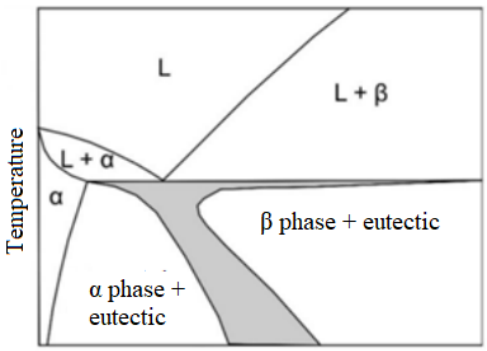

Figure 9. *Asymmetric coupled zone* (Stefanescu D, 2015)

It can be seen that supercooling, compared to the eutectic temperature, results in zones with different compositions. Thus, it is possible that the samples solidified with the slowest and fastest moving velocity were overcooled in a purely eutectic coupled zone, while the pieces with the medium moving speed were overcooled in the primary silicon + eutectic area.

The amount of eutectic in the samples increases along the entire length. The magnetic stirring was switched on halfway through the samples, which resulted in a visible decrease in the amount of the

eutectic. This may result from the secondary flow excited by the magnetic field as the amount of primary silicon in each piece increases before the mushy zone.

The average lamella distances were measured in 6 areas of the 5 samples with different movement velocities, as shown in *Figure 10*.

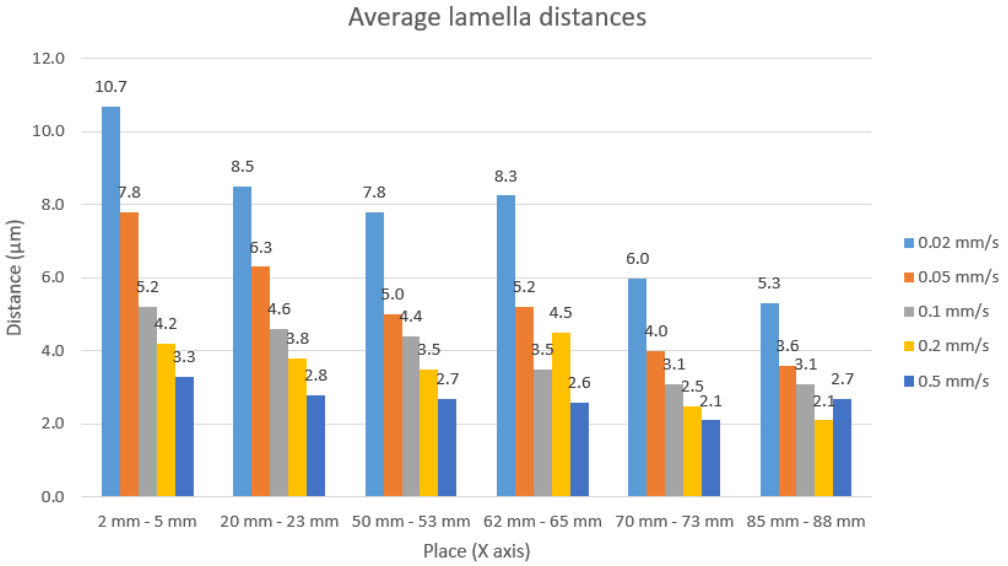

Figure 10. *Average lamella distances*

We can state that increasing the movement velocity definitely affects the fineness of the sample structure because the lamellas were, on average, the closest to each other in the piece that was moved the fastest [mm/s]. The stirring with 7.2 mT, did not have a particular effect on the lamella distances, as the values of the lamella distances show a characteristic decrease from the beginning to the end of the samples regardless.

When measuring the length of the eutectic silicon lamellas, we measured the longest eutectic lamellas of each sample, so we got the maximum lamella length values shown in *Figure 11*.

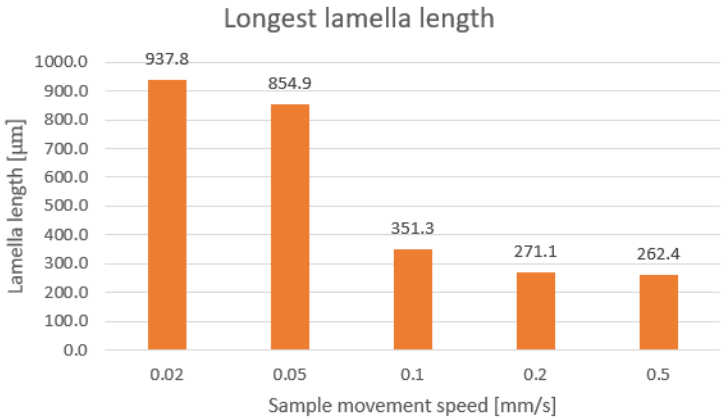

Figure 11. *Longest lamella length in the 5 samples*

We can say that shorter lamellas are formed by increasing the movement velocity. The difference between the longest eutectic lamellas of the samples, moved at a speed of 0.02 mm/s and 0.5 mm/s, is 675 μm. As a result, I calculated the frequency of lamellas under 10 μm in the samples, and the above finding is confirmed by the increase in the percentage of lamellae below 10 μm *(Figure 12)*.

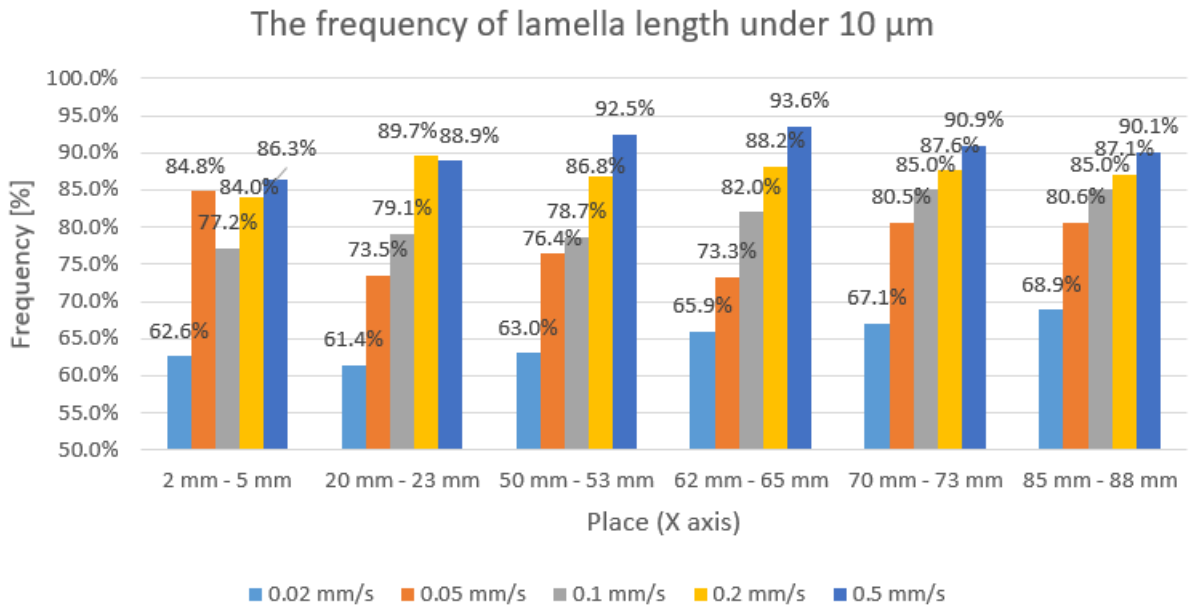

Figure 12. *Frequency of lamella length under 10 μm*

If we are interested in the fineness of the structure, it is worth investigating what the frequency of lamellas below 10 μm shows. In this case, we see a continuous increase in frequency, which increases not only due to the different movement velocities but also within the individual samples.

4. Conclusions

From the investigations, it can be concluded that both the stirring and the velocity of moving the sample affect the amount of eutectic and the length of the silicon lamellas in it. The amount of eutectic does not change significantly due to increasing the velocity, but at medium movement velocities, the amount of eutectic visibly decreases, which may be related to the asymmetric coupled zone. However, with RMF stirring, we can increase the amount of eutectic by an average of 8%, which can be favourable because cracks can start from large primary silicons.

The length of the silicon lamellas decreases due to increasing the movement velocity, and we can increase a large number of those under 10μm, thereby obtaining a finer structure. On average, it can be said that the proportions in the stirred and unstirred parts move together. So, by increasing the movement velocity, we definitely increase the number of shorter lamellas.

References

[1] Li, Y. Z., Mangelinck-Noel, N., Zimmermann, G., Sturz, L., & Nguyen-Thi, H. (2020). Modification of the microstructure by rotating magnetic field during the solidification of Al-7 wt.% Si alloy under microgravity. *Journal of Alloys and Compounds*, 836, 155458. **https://doi.org/10.1016/j.jallcom.2020.155458**

[2] Zimmermann, G. & Weiss, A. (2005). Directional solidification of dendritic microstructures in microgravity and with forced melt flow. *Microgravity – Science and Technology*, 16, 143–149. **https://doi.org/10.1007/BF02945965**

[3] Li, Y. Z., Mangelinck-Noel, N., Zimmermann, G., Sturz, L., & Nguyen-Thi, H. (2018). Effect of solidification conditions and surface pores on the microstructure and columnar-to-equiaxed transition in solidification under microgravity. *Journal of Alloys and Compounds*, 749, 344–354. **https://doi.org/10.1016/j.jallcom.2018.03.300**

[4] Miladinović, S., Stojanović, B., & Gajević, S. (2023). Hypereutectic aluminum alloys and composites: A review. *Silicon*, 15, 2507–2527. **https://doi.org/10.1007/s12633-022-02216-2**

[5] Matsuura, K., Kudoh, M. & Kinoshita, H. (2003). Precipitation of Si particles in a super rapidly solidified Al–Si hypereutectic alloy. *Materials chemistry and physics*, 81 (2–3), 393–395. **https://doi.org/10.1016/S0254-0584(03)00030-0**

[6] Pei, Y. & Hosson, J. D. (2001). Five-fold branched Si particles in laser clad AlSi functionally graded materials. *Acta Materialia*, 49 (4), 561–571. **https://doi.org/10.1016/S1359-6454(00)00364-5**

[7] Yi, H. & Zhang, D. (2003). Morphologies of Si phase and La-rich phase in as-cast hypereutectic Al–Si–xLa alloys. *Materials Letters*, 57 (16–17), 2523–2529. **https://doi.org/10.1016/S0167-577X(02)01305-8**

[8] Toropova, L. V., Alexandrov, D. V., Rettenmayr, M. & Liu, D. (2022). Microstructure and morphology of Si crystals grown in pure Si and Al–Si melts. *Journal of Physics: Condensed Matter*, 34. **https://doi.org/10.1088/1361-648X/ac3792**

[9] Day, M. G. & Hellawell, A. (1968). The microstructure and crystallography of aluminum-silicon eutectic alloys. *Mathematical Physical and Engineering Sciences*, 1408 (305), 473–491. **https://doi.org/10.1098/rspa.1968.0128**

[10] Holmes, A. M., Wang, X., Ma, N., Bliss, D. F. & Iseler, G. W. (2005). Vertical gradient freezing using submerged heater growth with rotation and with weak magnetic and electric fields. *International Journal of Heat and Fluid Flow*, 26 (5), 792–800. **https://doi.org/10.1016/j.ijheatfluidflow.2005.02.001**

[11] Cadirli, E., Kaya, H., Rabiger, D., Eckert, S. & Gündüz, M. (2015). Effect of rotating magnetic field on the microstructures and physical properties of Al–Cu–Co ternary eutectic alloy. *Journal of Alloys and Compounds*, 647, 471–480. **https://doi.org/10.1016/j.jallcom.2015.05.162**

[12] Chen, Z., Wen, X., Chen, C. (2010). Fluid flow and microstructure formation in a rotating magnetic field during the directional solidification process. *Journal of Alloys and Compounds*, 491(1–2), 395–401. **https://doi.org/10.1016/j.jallcom.2009.10.194**

[13] Veres, Zs., Roósz, A., Rónaföldi, A., Sycheva, A. & Svéda, M. (2022). The effect of melt flow induced by RMF on the meso- and micro-structure of unidirectionally solidified Al– 7wt.% Si alloy Benchmark experiment under magnetic stirring. *Journal of Materials Science & Technology*, 103, 197–208. **https://doi.org/10.1016/j.jmst.2021.06.060**

[14] Stefanescu, D. (2015). *Science and Engineering of Casting Solidification*. Springer. Cham. **https://doi.org/10.1007/978-3-319-15693-4**